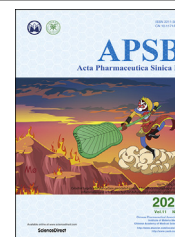




Chinese Pharmaceutical Association
Institute of Materia Medica, Chinese Academy of Medical Sciences

Acta Pharmaceutica Sinica B

www.elsevier.com/locate/apsb
www.sciencedirect.com



ORIGINAL ARTICLE

Targeting BMI-1-mediated epithelial–mesenchymal transition to inhibit colorectal cancer liver metastasis



Zhiyao Xu^{a,b,†}, Zhuha Zhou^{c,†}, Jing Zhang^a, Feichao Xuan^d, Mengjing Fan^{a,b}, Difan Zhou^d, Zhenyu Liuyang^d, Ximei Ma^d, Yiyang Hong^a, Yihong Wang^b, Sherven Sharma^e, Qinghua Dong^{a,f,*}, Guanyu Wang^{d,*}

^aBiomedical Research Center, Sir Run Run Shaw Hospital, School of Medicine, Zhejiang University, Hangzhou 310016, China

^bDepartment of Pathology, Sir Run Run Shaw Hospital, School of Medicine, Zhejiang University, Hangzhou 310016, China

^cDepartment of Gastrointestinal Surgery, the First Affiliated Hospital of Wenzhou Medical University, Wenzhou, 325000, China

^dDepartment of General Surgery, Sir Run Run Shaw Hospital, School of Medicine, Zhejiang University, Hangzhou 310016, China

^eDavid Geffen School of Medicine at UCLA, and the Veterans Affairs, Los Angeles, CA 90095, USA

^fKey Laboratory of Cancer Prevention and Intervention, China National Ministry of Education, Hangzhou 310009, China

Received 17 June 2020; received in revised form 7 September 2020; accepted 14 September 2020

KEY WORDS

BMI-1;
Colorectal cancer;

Abstract Liver is the most common metastatic site for colorectal cancer (CRC), there is no satisfied approach to treat CRC liver metastasis (CRCLM). Here, we investigated the role of a polycomb protein BMI-1 in CRCLM. Immunohistochemical analysis showed that BMI-1 expression in liver metastases was upregulated and associated with T4 stage, invasion depth and right-sided primary tumor. Knockdown

Abbreviations: ANOVA, One-way analysis of variance; CRC, colorectal cancer; CRCLM, colorectal cancer liver metastasis; EMT, epithelial–mesenchymal transition; HDACi, histone deacetylase inhibitor; HE, hematoxylin and eosin; IHC, immunohistochemistry; LNM, lymph node metastasis; NaB, sodium butyrate; PBS, phosphate buffered solution; PcG, polycomb-group; qPCR, real time polymerase chain reaction; TCGA, Cancer Genome Atlas.

*Corresponding authors. Tel./fax: +86 571 86006336.

E-mail addresses: wanguanyu@zju.edu.cn (Guanyu Wang), dongqinghua@zju.edu.cn (Qinghua Dong).

[†]These authors made equal contribution to this study.

Peer review under responsibility of Chinese Pharmaceutical Association and Institute of Materia Medica, Chinese Academy of Medical Sciences.

<https://doi.org/10.1016/j.apsb.2020.11.018>

2211-3835 © 2021 Chinese Pharmaceutical Association and Institute of Materia Medica, Chinese Academy of Medical Sciences. Production and hosting by Elsevier B.V. This is an open access article under the CC BY-NC-ND license (<http://creativecommons.org/licenses/by-nc-nd/4.0/>).

Liver metastasis;
Epithelial–mesenchymal
transition;
Snail;
AKT;
GSK-3 β ;
Sodium butyrate

BMI-1 in high metastatic HCT116 and LOVO cells repressed the migratory/invasive phenotype and reversed epithelial–mesenchymal transition (EMT), while *BMI-1* overexpression in low metastatic Ls174T and DLD1 cells enhanced invasiveness and EMT. The effects of *BMI-1* in CRC cells were related to upregulating snail *via* AKT/GSK-3 β pathway. Furthermore, knockdown *BMI-1* in HCT116 and LOVO cells reduced CRCLM using experimental liver metastasis mice model. Meanwhile, *BMI-1* overexpression in Ls174T and DLD1 significantly increased CRCLM. Moreover, sodium butyrate, a histone deacetylase and *BMI-1* inhibitor, reduced HCT116 and LOVO liver metastasis in immunodeficient mice. Our results suggest that *BMI-1* is a major regulator of CRCLM and provide a potent molecular target for CRCLM treatment.

© 2021 Chinese Pharmaceutical Association and Institute of Materia Medica, Chinese Academy of Medical Sciences. Production and hosting by Elsevier B.V. This is an open access article under the CC BY-NC-ND license (<http://creativecommons.org/licenses/by-nc-nd/4.0/>).

1. Introduction

Colorectal cancer (CRC) is the third most common cancer diagnosed among men and women and the second leading cause of cancer death in the world^{1,2}. Metastatic or recurrent disease is the most common cause of death in CRC patients. The liver plays a pivotal role in the survival of patients with CRC and often is the only site of metastases. About 14%–35% of patients diagnosed with CRC present liver metastases at diagnosis and 70% of patients with CRC will develop liver metastases during their disease process. Patients with untreated CRC liver metastases (CRCLM) have a median survival of 5–12 months³. Despite extensive research into the biology of CRC progression, the molecular mechanisms involved in CRCLM are not well characterized. Thus, finding a new pivotal molecule in CRCLM is important for the development and optimal use of novel anticancer therapies.

BMI-1 belongs to the polycomb-group (PcG) protein family members. As a key transcriptional repressor, *BMI-1* negatively regulates the *Ink4a/Arf* locus that encodes two tumor suppressor proteins, p16^{INK4a} and p19^{ARF}⁴. *BMI-1* is involved in controlling stem cell self-renewal and carcinogenesis of a number of human cancers, such as CRC⁵. *BMI-1* is overexpressed in a variety of different types of human tumor and is related to progression and poor prognosis. *BMI-1* expression in CRC tissue is significantly higher than healthy colon tissue, high *BMI-1* expression is associated with poor overall survival in CRC patients^{6–8}. The level of cell-free *BMI-1* mRNA is increased in serum of CRC patients and may be a potential marker for early diagnosis and prognostic prediction of CRC⁹. The mRNA expression level of plasma *BMI-1* may be a potential prognostic biomarker for distant metastasis in CRC patients¹⁰. *Bmi-1* deficiency in mice impairs the progression and maintenance of small intestinal tumors in a cell autonomous and highly *Arf*-dependent manner¹¹. *BMI-1* knockdown in human CRC cell lines suppresses cell proliferation *in vitro* and xenografts¹². Recently, study found that CRCs with liver metastases significantly acquired mutations in *BMI-1* (3 of 34 patients)¹³. However, the role of *BMI-1* in the progression of CRCLM remain largely unknown.

The goal of our current study is to investigate whether *BMI-1* overexpression would contribute to facilitate formation of CRCLM *in vitro* and *in vivo*. Clinically, we found that *BMI-1* was significantly higher expressed in a cohort of human hepatic metastases (but not lymph node metastases) than in their primary colorectal tumors. *BMI-1* expression in liver metastases was significantly associated with a higher T stage, invasion depth and primary tumor position (right-sided tumor) at diagnosis of the

primary tumor. *BMI-1* regulates metastatic phenotypes in CRC cell lines by modulating snail-mediated epithelial–mesenchymal transition (EMT). The effect of *BMI-1* on liver metastatic potential was also confirmed using *in vivo* experimental liver metastasis mice model. Moreover, sodium butyrate (NaB), a *BMI-1* inhibitor, reduced HCT116 and LOVO liver metastases in mice. Therefore, *BMI-1* appears to play a critical role in the establishment of CRCLM and maybe an effective target for treatment of CRCLM.

2. Methods and materials

2.1. Patients and samples

A total of 98 formalin fixed paraffin embedded tissues that encompass primary CRC (38 cases), paired metastatic liver (38 cases) and metastatic lymph node (22 cases) from 38 CRC patients with clinic diagnoses were collected from the Department of Pathology (from 2006 to 2019), Sir Run Run Shaw Hospital, Hangzhou, China. The slides were stained with primary antibody for *BMI-1* (1:150; Millipore Inc., Billerica, MA, USA) overnight at 4 °C and followed by secondary antibody incubation. Specimens were analyzed under a light microscope. Patients who met the following criteria were enrolled: 1) histologically confirmed colorectal adenocarcinoma, 2) metastases limited to the liver before liver resection, 3) R0 resection for primary lesion and metastases. Patient characteristics are given in Supporting Information Table S1.

Immunohistochemistry (IHC) interpretation was performed by a semi-quantitative scoring method and evaluated by two independent pathologists. Nuclear staining was considered positive for *BMI-1*. The score was reached by multiplying the percentage of positive tumor cells (*P*) by the intensity of staining (*I*). The value of *P* was defined as 0 (no staining), 1 (0%–25%), 2 (25%–50%) and 3 (>50%). The value of *I* was defined as 0 (negative), 1 (weakly positive), 2 (positive) and 3 (strong positive). The tumor tissues were categorised into three groups according to the score: low, score ≤ 3 ; middle, score 4–6; high: score 7–9.

Primary CRC tumor and paired metastatic liver tissue samples were obtained from 11 CRC patients undergoing tumor resection at the Sir Run Run Shaw Hospital of Zhejiang University. Patients who received pre-operative chemotherapy were excluded. The biopsies were snap-frozen in liquid nitrogen and stored at -80 °C until use.

This study was performed in strict accordance with the recommendations from the Guide for Clinical Research provided by Sir Run Run Shaw Hospital, Zhejiang University. The protocol

was approved and monitored by the Ethics Committee of Sir Run Run Shaw Hospital, Zhejiang University. Informed consent was obtained from all patients.

2.2. Cell culture and treatment

Four human CRC cell lines, including two high metastatic CRC cell lines (LOVO and HCT116) and two low metastatic CRC cell lines (Ls174T and DLD1) were obtained from the American Type Culture Collection (Manassas, VA, USA). Cells were cultured in the recommended growth medium, namely F12K, McCoy's 5A (GENOM, Hangzhou, China) and Dulbecco's modified Eagle's medium (Gibco, Life Technologies Inc., Grand Island, NY, USA), respectively, with 10% fetal bovine serum in a humidified incubator at 37 °C with 5% CO₂. Lentiviral constructs for wild type BMI-1 overexpression (pGC-FU-GFP-BMI-1 and pGC-FU-GFP control) and knockdown (p-GCSIL-GFP-shBMI-1 and p-GCSIL-GFP control) were purchased from Genechem (Shanghai, China). Cells were infected with the lentivirus and selected by puromycin according to the manufacturer's instructions.

2.3. Real time polymerase chain reaction (qPCR)

Total tissue RNA was purified using TRIzol reagent (Invitrogen) and reverse transcribed using a reverse transcription system (Promega, Madison, WI, USA), according to the manufacturer's instructions. BMI-1, EZH2, snail and GAPDH were subjected to qPCR in triplicates for each sample using FastStart Universal SYBR Green Master (Roche Diagnostics, Rotkreuz, Switzerland), and results analyzed with a 7500 Real-Time PCR system (Applied Biosystems by Life Technologies). The primer sequences were obtained from the Universal Probe Library (Roche). The 2^{-ΔΔCt} value determination method was used to compare the fold differences in expression.

2.4. Immunoblotting and immunofluorescence staining

Cells were washed with phosphate buffered solution (PBS) and whole cell lysate was prepared with modified RIPA buffer. Supernatants of the homogenates were subjected to 4%–12% Bis-Tris gel by electrophoresis, and transferred to PVDF membranes. The membranes were probed with anti-vimentin, anti-GAPDH, anti-rabbit or mouse IgG horseradish peroxidase (Sigma, St. Louis, MO, USA), anti-BMI-1 (Millipore Inc., Billerica, MA, USA), anti-AKT, anti-p-AKT (Santa Cruz Biotechnology, Santa Cruz, CA, USA), anti-GSK3b, anti-p-GSK3b, anti-snail, anti-α-catenin, anti-β-catenin (Cell Signaling Technology, Beverly, CA, USA) and detected with ECL Western blotting detection reagents (Thermo Fisher, Palo Alto, CA, USA).

Immunofluorescence staining was performed on cells plated in chamber slides. The cells were fixed in 3.7% formaldehyde for 15 min, washed three times with PBS and permeabilized with 0.25% Triton X-100 in PBS for 10 min. Mouse monoclonal anti-snail, anti-vimentin, and Alex Fluor®568 goat anti-mouse IgG (Millipore Inc.) were used as primary and secondary antibodies, respectively. Images were obtained using a Zeiss LSM 710 confocal microscope system (Carl Zeiss, Jena, Germany).

2.5. Transwell migration assay

Cells (6 × 10⁴) in serum free medium were plated into the upper chambers of transwells (Corning, NY, USA) and medium with

10% fetal bovine serum was placed in the lower chambers for 48 h in 37 °C in a humidified incubator at 37 °C with 5% CO₂. The cells remaining in the upper chamber were carefully removed by cotton swab, and the cells migrated to the lower membrane surface were fixed in 4% paraformaldehyde and stained with crystal violet. The cells were counted in five randomly selected microscopic fields (100×) in each experiment. Each sample was run in triplicate and the experiments were repeated three times.

2.6. Wound healing assay

Cells were seeded in 6-well plates until they reached 90% confluence. The cells were then serum starved for 24 h, and a linear wound was created in the confluent monolayer using a pipette tip. Wounds were observed and photographed digitally using an inverted Olympus IX50 microscope with 10× objective lens at various times as indicated in the figure legends. Wound size was measured randomly at five sites perpendicular to the wound.

2.7. Experimental liver metastasis model

All animal care and experimental procedures were in strict accordance with the recommendations in the Guide for the Care and Use of Laboratory Animals of Zhejiang University and were approved by the Committee on the Ethics of Animal Experiments of Zhejiang University.

2.7.1. Treatment protocol 1

BALB/c nude mice (male, 5-week-old, 17–18 g) were randomly grouped on the basis of body weight by the stratified randomization method. For HCT116 and LOVO cells, the number of mice was 7 in each group. For Ls174T and DLD1 cells, the number was 10. Mice were anesthetized with 1% pentobarbital sodium (40 mg/kg, i.p.) and the spleen was exteriorized through a left lateral flank incision. Tumors were established by intrasplenic injection of 2 × 10⁶ CRC cells suspended in 100 μL of serum-free growth media using a 27-gauge needle. The injection site on the spleen was pressed with a cotton stick wet in iodine-povidone solution for 5 min. The peritoneum and skin were closed in a single layer with surgical thread. Three weeks after HCT116 and LOVO cells inoculation, or six weeks after Ls174T and DLD1 cells inoculation, mice were sacrificed and metastatic tissues were examined. Visible liver metastatic nodule larger than 1 mm in diameter was counted. Resected livers were fixed for IHC. Liver tissues were also collected for Western blot assay.

2.7.2. Treatment protocol 2

NaB was purchased from Sigma. The mice were treated with NaB (200 mg/kg/day, once daily, i.g.; *n* = 7) or saline (i.g., *n* = 7) 7 days before CRC cells (HCT116 or LOVO) intrasplenically transplantation. Subsequently, NaB were administered once each day for 21 days. One mouse died in HCT116 control group. Three weeks after inoculation, mice were sacrificed by carbon dioxide inhalation and metastatic tissues were examined in paraffin-embedded sections.

2.7.3. IHC

Tumor tissue samples were fixed in 10% formalin for 24 h, embedded in paraffin, cut in 5 μm sections, stained with Harris Hematoxylin & Eosin and evaluated for structural changes under a bright field microscope. Standard immunoperoxidase procedures were used to visualize BMI-1 and snail in tumor samples. Briefly, sections were deparaffinized, blocked with goat serum,

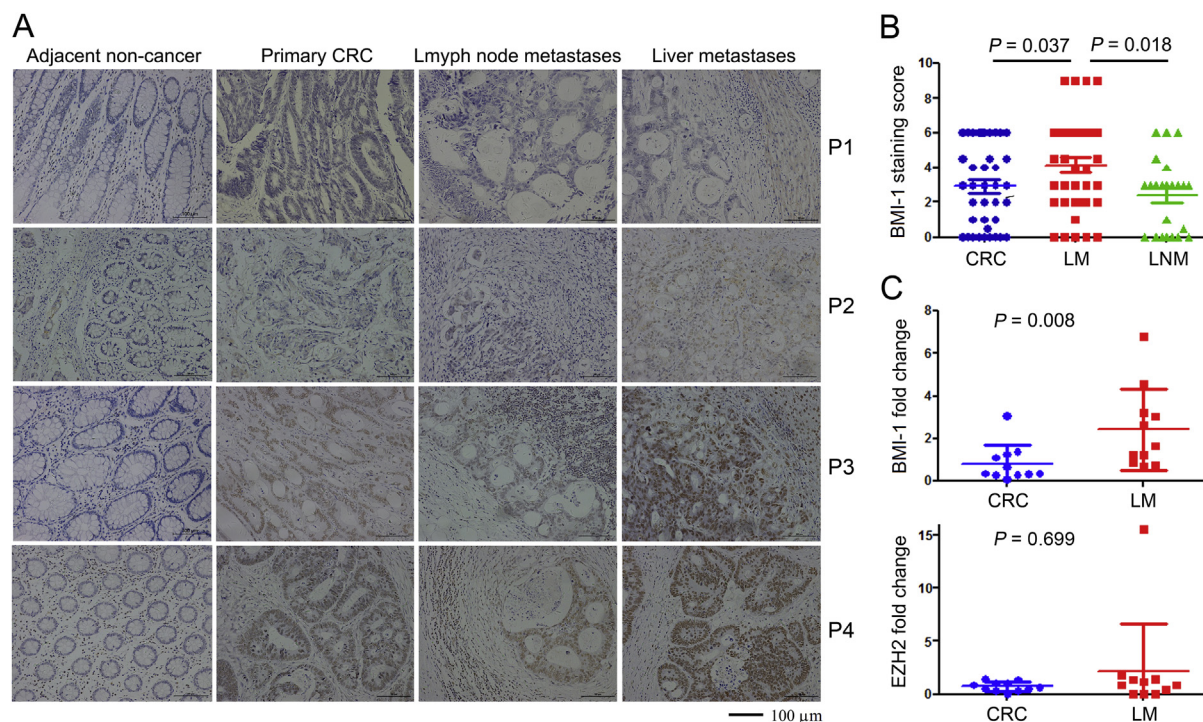


Figure 1 Expression of BMI-1 in human CRC primary and metastatic tumors. (A) Immunohistochemical staining of BMI-1 in paired tissue samples from four CRC patients (P1–P4). (B) Immunoreactivity scores in primary CRC (CRC), liver metastases (LM), lymph node metastases (LNM). (C) Real-time PCR quantification of *BMI-1* mRNA expression levels in human CRC primary and liver metastatic tumors. *BMI-1* and *EZH2* expression levels are presented as the fold changes relative to that in primary tumor and normalized to *GAPDH*. *BMI-1* is upregulated in CRC liver metastases.

followed by incubation with anti-BMI-1 (1:150) or anti-snail (1:100) overnight at 4 °C. After incubation with horseradish peroxidase linked secondary antibody for 30 min, the sections were counterstained with Mayer's hematoxylin.

2.8. Statistical analysis

All the clinic statistical analysis was performed with R software (version: 3.6.3), and statistical tests under Kruskal–Wallis and Fisher's exact test. Results are expressed as mean \pm standard error of mean (SEM). One-way analysis of variance (ANOVA) for multiple comparisons was used to detect differences amongst the various treatments. Once significant differences were detected ($P < 0.05$), Student's two-tailed *t*-test or Mann–Whitney test was used to evaluate the differences between two groups. The correlations in the gene expression levels were analysed by Pearson's correlation coefficient.

3. Results

3.1. *BMI-1* is overexpressed in liver metastases of human colorectal cancer

We analyzed the BMI-1 expression level in a cohort of 41 normal subjects and 288 CRC from the Cancer Genome Atlas (TCGA) database, the result showed that BMI-1 was upregulated in CRC (Supporting Information Fig. S1). We then

performed IHC analysis to evaluate the expression level of BMI-1 protein in primary CRC tissues, paired liver metastases and lymph node metastases (LNM). Consistent with previous reports^{6–8}, BMI-1 staining was negative or weak in the nucleus of non-cancerous colorectal mucosal epithelial cells (Fig. 1A). In primary CRC tissues, the positivity of BMI-1 expression was 78.9% (30 among 38 samples), the score of BMI-1 expression was not significantly associated with clinicopathological characteristics (including differentiation, T stage, N stage) except BMI-1 expression level in liver metastases (Table S1). In the paired LNM, the expression level of BMI-1 was almost the same as the primary CRC, the score of BMI-1 expression was not significantly associated with clinicopathological characteristics except BMI-1 expression level in primary CRC (Supporting Information Table S2). Interestingly, the expression level of BMI-1 in the paired liver metastases was significantly enhanced (Fig. 1A and B), and significantly associated with primary tumor position (right-sided tumor), tumor invasion depth and clinic T4 stage (Table 1).

To evaluate the expression level of *BMI-1* mRNA in liver metastases of human CRC, we performed qPCR across a total of 22 tissues that encompass primary CRC, paired metastatic liver from 11 CRC patients (Fig. 1C). Our results also exhibit that *BMI-1* expression level was significantly higher in liver metastases. We also checked the expression level of *EZH2*, another pivotal PcG family number. There was no significant difference between primary CRC and liver metastases. These data demonstrate that BMI-1 is overexpressed in CRC liver metastatic tumors.

Table 1 Correlation between CRC patient clinicopathological characteristics and BMI-1 expression in liver metastases.

Characteristic	BMI-1 expression in liver metastases				P-value ^b
	Overall (n = 38)	Low (n = 16, 42%) ^a	Middle (n = 18, 47%) ^a	High (n = 4, 11%) ^a	
Age	59 (54, 68)	58 (52, 71)	58 (55, 66)	67 (64, 69)	0.520
Gender					0.410
Female	16 (42%)	7 (44%)	6 (33%)	3 (75%)	
Male	22 (58%)	9 (56%)	12 (67%)	1 (25%)	
Primary tumor					0.130
Colon	17 (45%)	8 (50%)	5 (28%)	4 (100%)	
Rectum	13 (34%)	4 (25%)	9 (50%)	0 (0%)	
Sigmoid	8 (21%)	4 (25%)	4 (22%)	0 (0%)	
Primary tumor position ^c					0.003
Left-sided tumor	21 (55%)	8 (50%)	13 (72%)	0 (0%)	
Right-sided tumor	17 (45%)	8 (50%)	5 (28%)	4 (100%)	
Differentiation					0.100
Well	7 (18%)	6 (38%)	1 (5.6%)	0 (0%)	
Well-moderate	17 (45%)	6 (38%)	10 (56%)	1 (25%)	
Moderate	6 (16%)	1 (6.2%)	4 (22%)	1 (25%)	
Poor	5 (13%)	2 (12%)	1 (5.6%)	2 (50%)	
Unknown	3 (7.9%)	1 (6.2%)	2 (11%)	0 (0%)	
Morphology					0.450
Infiltrative	3 (7.9%)	3 (19%)	0 (0%)	0 (0%)	
Protrusive	3 (7.9%)	2 (12%)	1 (5.6%)	0 (0%)	
Ulcerative	27 (71%)	9 (56%)	14 (78%)	4 (100%)	
Protrusive/ulcerative	5 (13%)	2 (12%)	3 (17%)	0 (0%)	
Invasion					0.027
Muscularis	2 (5.3%)	0 (0%)	2 (11%)	0 (0%)	
Serosa	13 (34%)	5 (31%)	4 (22%)	4 (100%)	
Pericolonic	23 (61%)	11 (69%)	12 (67%)	0 (0%)	
Primary CRC (max)					0.240
<5 cm	25 (66%)	11 (69%)	13 (72%)	1 (25%)	
≥5 cm	13 (34%)	5 (31%)	5 (28%)	3 (75%)	
Clinical T stage					0.012
T3	35 (92%)	15 (94%)	18 (100%)	2 (50%)	
T4	3 (7.9%)	1 (6.2%)	0 (0%)	2 (50%)	
Clinical N stage					0.190
N0	9 (24%)	3 (19%)	6 (33%)	0 (0%)	
N1	17 (45%)	5 (31%)	9 (50%)	3 (75%)	
N2	12 (32%)	8 (50%)	3 (17%)	1 (25%)	
BMI-1 expression in primary CRC					<0.001
Low	22 (58%)	15 (94%)	6 (33%)	1 (25%)	
Middle	16 (42%)	1 (6.2%)	12 (67%)	3 (75%)	
High	0 (0%)	0 (0%)	0 (0%)	0 (0%)	
Lymph node metastasis ratio	0.13 (0.01, 0.33)	0.28 (0.06, 0.40)	0.05 (0.00, 0.20)	0.11 (0.08, 0.18)	0.310
Liver metastasis (max)					0.130
<5 cm	30 (79%)	10 (62%)	16 (89%)	4 (100%)	
≥5 cm	8 (21%)	6 (38%)	2 (11%)	0 (0%)	
Liver metastasis number					0.990
Multiple	21 (55%)	9 (56%)	10 (56%)	2 (50%)	
Single	17 (45%)	7 (44%)	8 (44%)	2 (50%)	
Synchronous liver metastasis					0.055
Yes	7 (18%)	3 (19%)	2 (11%)	2 (50%)	
No	11 (29%)	2 (12%)	9 (50%)	0 (0%)	
Unknown	20 (53%)	11 (69%)	7 (39%)	2 (50%)	

^aStatistics presented: median (IQR); n (%).^bStatistical tests performed: Kruskal–Wallis test; Fisher's exact test.^cAccording to embryologic origin.

Thus, the overexpression of BMI-1 was related to liver metastases of CRC, but not lymph node metastases of CRC.

3.2. *BMI-1 enhances migration and the EMT phenotype of CRC cells*

To investigate the effect of BMI-1 on CRC cell migration, we stably knocked down its expression using lentiviral shRNA in two high liver metastatic CRC cell lines, HCT116 and LOVO. Two low liver metastases CRC cell lines, Ls174T and DLD1, stably overexpressing BMI-1 were also established (Fig. 2F). As shown in Fig. 2A, *BMI-1* knockdown in HCT116 and LOVO cells caused significant reduction in colony number. Ectopic expression of BMI-1 significantly increased colony formation in Ls174T and DLD1 cells. We then investigated the effect of BMI-1 on the aggressive phenotype of CRC cells. Transwell migration assay (Fig. 2B) and wound healing assays (Fig. 2C and D) demonstrated that *BMI-1* knockdown significantly decreased the rate of migration in high metastatic HCT116 and LOVO cells, as compared with that of control cells. Overexpression of BMI-1 significantly increased the rate of migration in low metastatic Ls174T and DLD1 cells. We further investigated the impact of BMI-1 on EMT, which is an important process in tumor progression. *BMI-1* knockdown HCT116 cells showed a typical cuboidal epithelial shape by immunofluorescent staining, meanwhile BMI-1 overexpressed DLD1 cells were elongated and larger than control cells (Fig. 2E). In order to determine whether *BMI-1* knockdown inhibits EMT, we probed the cells with epithelial and mesenchymal markers. *BMI-1* knockdown in HCT116 cells inhibited the typical EMT phenotype, increased epithelial markers α -catenin and downregulated mesenchymal marker vimentin. While BMI-1 overexpressed in DLD1 cells decreased α -catenin and increased vimentin (Fig. 2E and F). We also examined the expression level of snail, an EMT-related transcription factor. *BMI-1* knockdown in HCT116 cells obviously decreased snail expression by immunofluorescent staining and WB. Meanwhile, snail was upregulated in BMI-1 overexpressed DLD1 cells (Fig. 2E and F). The same phenomena were observed in *BMI-1* knockdown LOVO cells and BMI-1 overexpressed Ls174T cells (Fig. 2F), which confirmed that BMI-1 played an important role in CRC EMT process. Therefore, we determined that BMI-1 is essential for malignant transformation of CRC cells.

3.3. *BMI-1 regulates snail expression through AKT/GSK-3 β signaling in CRC cells*

Previous studies indicated that AKT/GSK-3 β /snail signal pathway is importantly involved in metastasis by modulating EMT process¹⁴, we examined the expression level of several proteins involved in this signaling pathway. As shown in Fig. 3A, BMI1 did not change the total amount of AKT and GSK-3 β in CRC cells, whereas AKT phosphorylation was inhibited in *BMI-1* knockdown HCT116 and LOVO cells, and accompanied by decrease in phosphorylation of GSK-3 β and downregulation of β -catenin, a downstream target protein of GSK-3 β . Meanwhile, upregulation of BMI-1 in Ls174t and DLD1 cells activated the AKT/GSK-3 β / β -catenin pathway (Fig. 3A). To investigate whether the induction of EMT were caused by activation of the PI3K/AKT/GSK-3 β pathway, we used the PI3K inhibitor wortmannin. Wortmannin treatment reversed the increase in E-cadherin, phosphorylation of AKT and GSK-3 β , and leading to the decrease in snail to the level presented in control DLD1 cells (Fig. 3B). To determine the role of snail in BMI-1-mediated

metastasis in CRC, HCT116 cells transfected with sh-*BMI-1* plus Lv-snail and DLD1 cells transfected with Lv-*BMI-1* plus sh-snail were used to perform further experiments. Snail overexpression decreased expression of E-cadherin and increased expression of vimentin (Fig. 3C), also rescued the migration inhibited by *BMI-1* knockdown (Fig. 3D). However, snail knockdown increased expression of E-cadherin and decreased expression of vimentin (Fig. 3C), also significantly reduced BMI-1-enhanced cell migration (Fig. 3D). These results demonstrate that BMI-1 promoted CRC EMT at least partly by upregulating snail expression *via* activating AKT/GSK-3 β pathway. These results suggest that BMI-1 regulated EMT through AKT/GSK-3 β /snail pathway.

3.4. *BMI-1 is positive correlated with snail in CRC tissues*

We further investigated the correlation between the expression level of BMI-1 and snail. Real-time PCR analysis in primary CRC tissues and paired liver metastases showed that the mRNA expression levels of *BMI-1* and snail were positive correlated (Fig. 4A). We also detected the protein levels of BMI-1 and snail in paired tissues from 5 CRC patients. The protein levels of BMI-1 and snail were coincidentally. Tumor tissues expressed higher BMI-1 and snail than non-cancerous tissues, liver metastases expressed higher BMI-1 and snail than primary CRC tumors (Fig. 4B). These results suggest that BMI-1 may regulate snail in CRC progression.

3.5. *BMI-1 is critical for metastasis of CRC cells in a CRC liver metastatic xenograft model*

To assessed the role of BMI-1 in the establishment of colorectal cancer metastases, we tested the metastatic behavior of CRC cells overexpressed BMI-1 or *BMI-1* knockdown. Three weeks after injection, all the mice formed tumors in spleen, and 100% mice injected with HCT116 sh-Control and LOVO sh-Control cells formed surface liver metastases, while 3 of 7 mice injected with HCT116 sh-*BMI-1*, 2 of 7 mice injected with LOVO sh-*BMI-1* cells formed liver metastases (Fig. 5A and B). The numbers of metastatic nodules in the livers were significantly reduced in mice injected with HCT116 sh-*BMI-1* and LOVO sh-*BMI-1* cells compared with the numbers in those injected with HCT116 sh-Control and LOVO sh-Control cells (Fig. 5B). Meanwhile, six weeks after injection, 4 of 10 mice injected with DLD1 vector cells, 3 of 10 mice injected with Ls174T vector cells formed surface liver metastases. BMI-1 overexpression significantly increased liver metastases, 8 of 10 mice injected with DLD1 *BMI-1* and 10 of 10 mice injected with Ls174T *BMI-1* cells formed surface liver metastases and the number of surface metastases per liver was also significantly increased (Fig. 5B). We used IHC to measure BMI-1 and snail expression in metastatic liver tissues. The staining of BMI-1 and snail in HCT116 sh-Control cells injected mouse liver were much stronger than that of HCT116 sh-*BMI-1* cells injected mice liver, while BMI-1 and snail expression in DLD1 vector cells injected mouse liver were obviously reduced compared to that of DLD1 *BMI-1* cells injected mouse liver (Fig. 5C). Western blot results also confirmed that the expression levels of BMI-1 and snail were reduced in HCT116 sh-*BMI-1* cells injected mice livers, and increased in DLD1 *BMI-1* cells injected mouse livers (Fig. 5D). Together, these results suggest that BMI-1 is essential for efficient execution of the metastatic program.

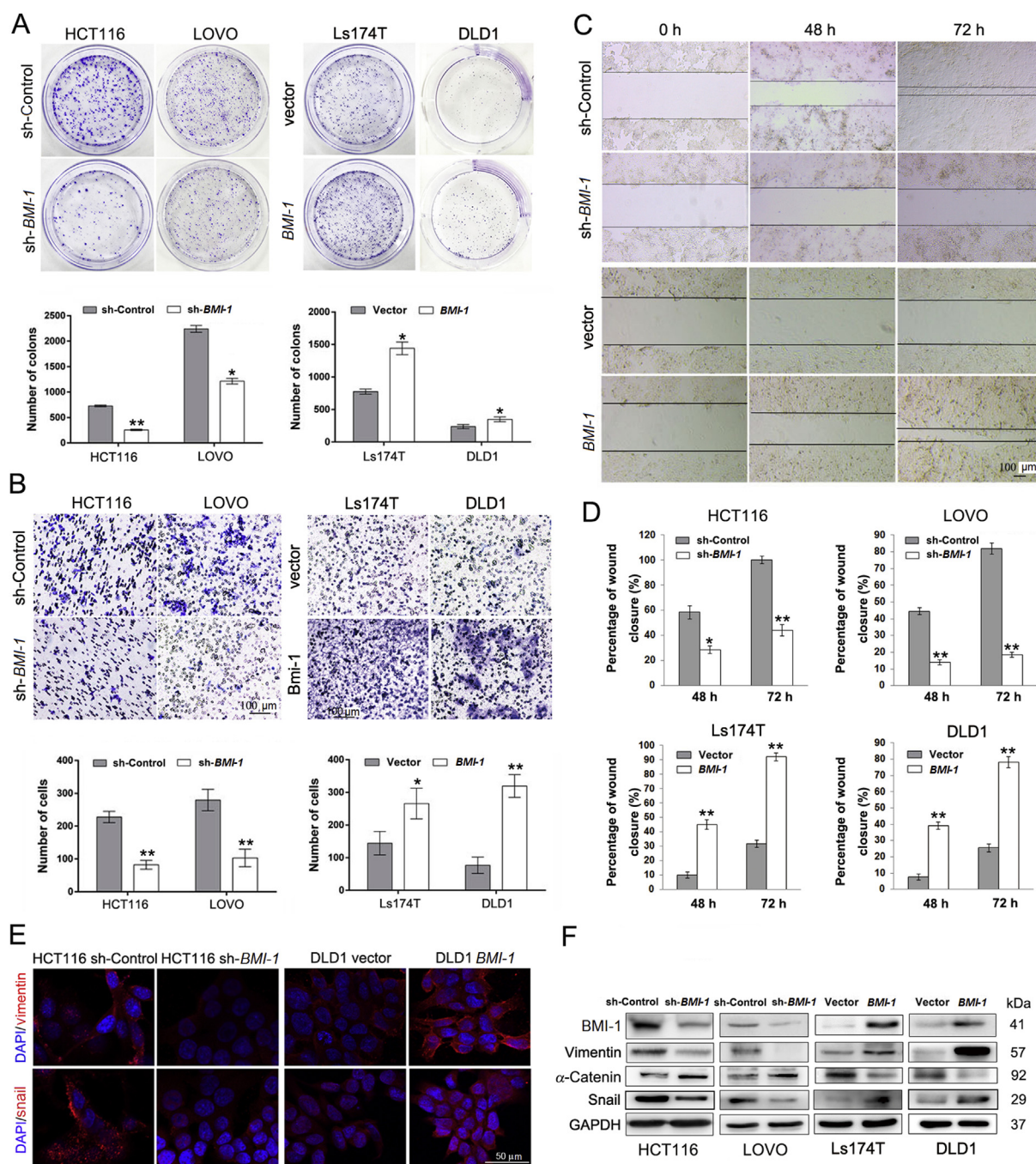


Figure 2 BMI-1 is essential for malignant transformation of CRC cells. (A) *BMI-1* knockdown significantly inhibited colony formation. *BMI-1* was knocked down using lentiviral shRNA in HCT116 and LOVO cells. Cells were seeded in 6-well plate, colony formation was observed after 7 days. Data are presented as mean \pm SD; * $P < 0.05$, ** $P < 0.01$ vs. control cells. (B) Representative micrographs and quantification of cell migration in the transwell migration assay (without matrigel). Migrated cells were plotted as the average number of cells per field of view from 3 different experiments, as described in Methods. Scale bar: 100 μ m. Data are presented as mean \pm SD; ** $P < 0.01$ vs. control cells. (C) *BMI-1* knockdown significantly inhibited cell migration. The migration properties of the cells were analyzed in LOVO cells by wound healing assay. Cells were grown to confluent on 6-well plates. A scratch was made through the cell layer using a pipette tip. Photographs of the wounded area ($n = 3$) were taken immediately after the scratch was made (0 h) and 48 or 72 h later in order to monitor cell movement into the wounded area. Scale bar: 100 μ m. Data are presented as mean \pm SD; * $P < 0.05$, ** $P < 0.01$ vs. control cells (Student's *t*-test). (D) Quantification of cell migration in the sh-Control and sh-*BMI-1* CRC cells. (E) CRC cells were replated on coverslips. After an additional 24 h, cells were stained for vimentin and snail, then analyzed by confocal microscopy. The red signal represents staining for the corresponding protein, while the blue signal signifies nuclear DNA staining with DAPI. Scale bar: 50 μ m. (F) Expression of the epithelial proteins α -catenin, the mesenchymal protein vimentin, and snail in CRC cells were detected by Western blot analysis. GAPDH was used as a loading control.

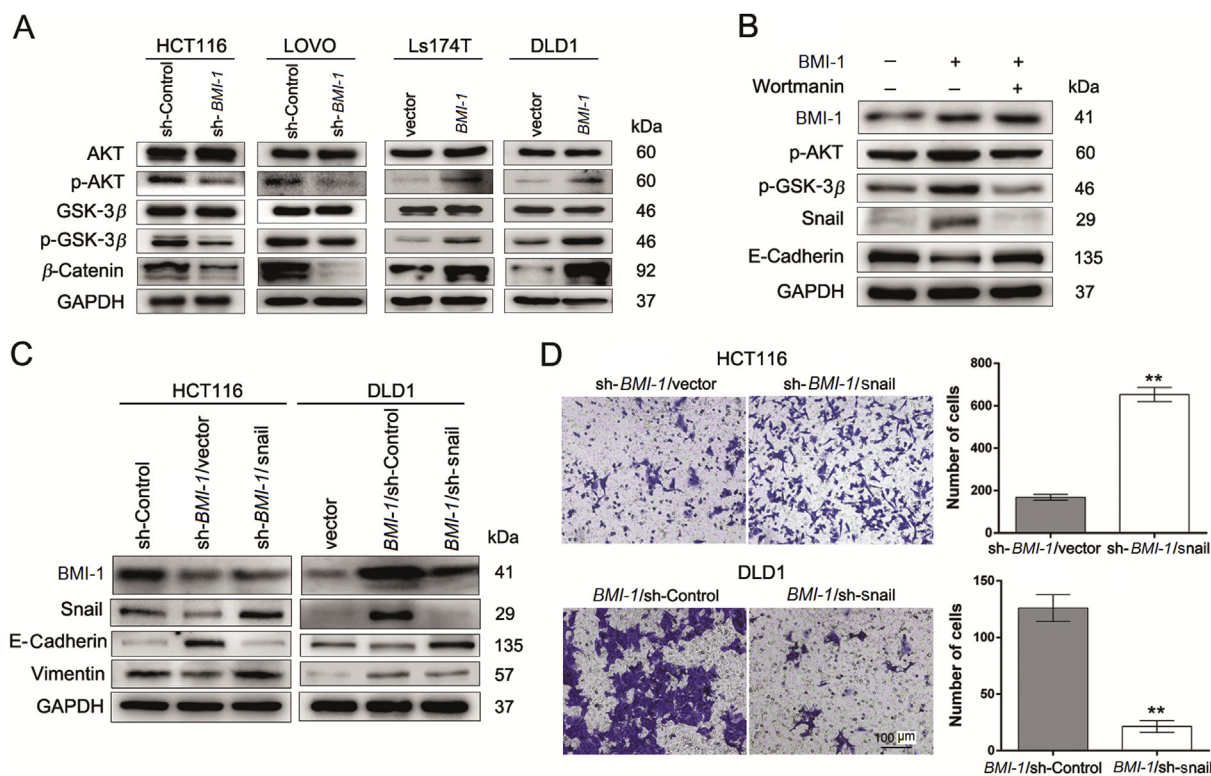


Figure 3 BMI-1 upregulates snail expression. (A) Western blot analysis of the indicated proteins involved in AKT/GSK-3 β signaling. (B) PI3K inhibitor wortmannin treatment inhibited BMI-1-activated AKT/GSK-3 β /snail signaling in DLD1 cells. (C) Western blot analysis of BMI-1, snail, E-cadherin, and vimentin. GAPDH was used as a control. Snail knockdown significantly decreased BMI-1-enhanced EMT, while snail overexpression promoted *BMI-1* knockdown inhibited EMT. (D) Representative images and corresponding statistical analysis of transwell assay. Migrated cells were plotted as the average number of cells per field of view from 3 different experiments. *BMI-1* knockdown inhibited CRC cells migration, while BMI-1 overexpression promoted migration. Scale bar: 100 μ m. Data are presented as mean \pm SD; ** P < 0.01 vs. control cells.

3.6. *BMI-1* inhibitor sodium butyrate reduces CRC liver metastasis *in vivo*

Sodium butyrate (NaB) is one of the histone deacetylase inhibitors (HDACi), which participate in chromatin remodeling by reprogramming the acetylation status of histones and nonhistone proteins¹⁵. BMI-1 is a transcriptional target of HDACi¹⁶. Our previous data confirmed that NaB inhibited BMI-1 expression in CRC cells *in vitro* and *in vivo*¹⁷. We further investigate the effect of BMI-1 inhibitor NaB on CRC liver metastasis. 6 of 6 mice (7

mice per group, one mouse died after surgery) injected with HCT116 formed surface liver metastases in control group, among them 5 mice had malignant ascites. Meanwhile, only 5 of 7 in NaB treated mice formed liver metastases and 2 of 7 had malignant ascites (Fig. 6A). NaB treatment also reduced liver metastases in mice injected with LOVO cells from 7/7 to 2/7. NaB treatment significantly reduced the number of surface metastases per liver both in mice injected with HCT116 and LOVO cells (Fig. 6B). IHC and Western blot results showed that BMI-1 expression in liver metastasis was reduced after NaB treatment, snail expression

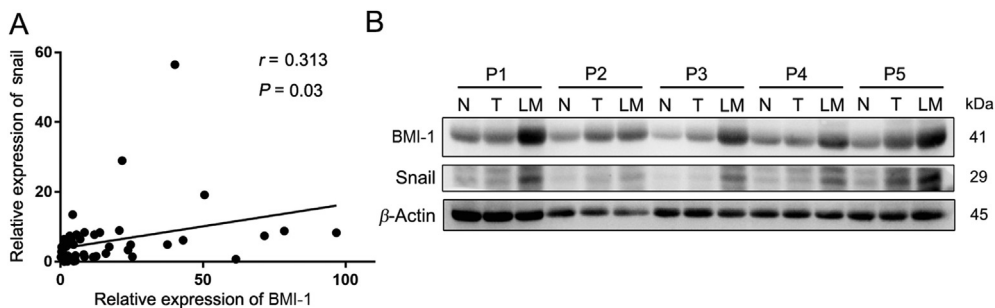


Figure 4 BMI-1 was positive correlated with snail in CRC tissues. (A) A clear positive correlation was observed between *BMI-1* and snail in human CRC tissues. (B) BMI-1 expression in paired tissues from 5 CRC patients was detected by Western blot analysis. β -Actin was used as a control. N, non-cancerous tissues; C, primary CRC tissues; LM, liver metastases.

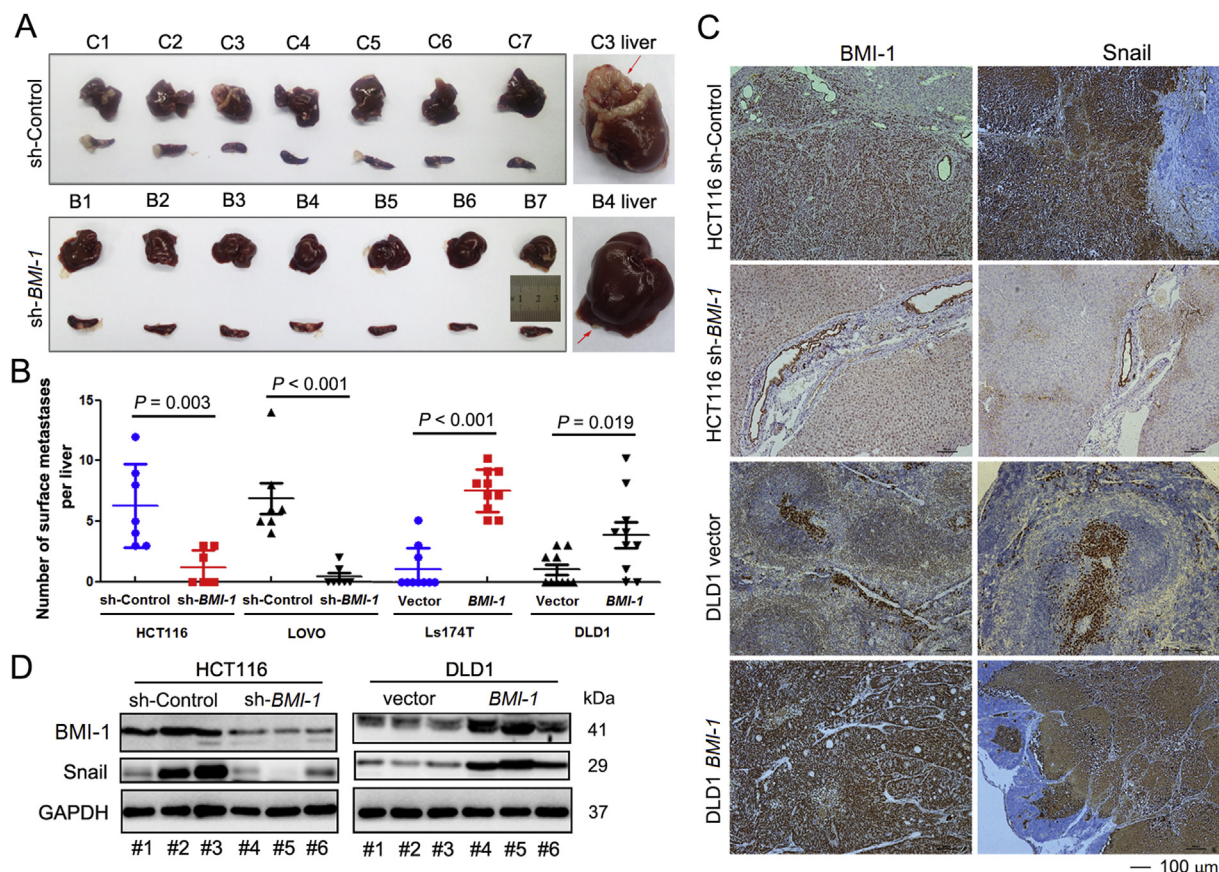


Figure 5 BMI-1 promoted CRC liver metastasis *in vivo*. (A) Representative images of spleen and liver in nude mice injected with LOVO sh-Control or LOVO sh-BMI-1 cells ($n = 7$ per group). Three weeks after injection of the transfected cells into the spleens of athymic nude mice, animals were killed and livers were examined for metastatic nodules. The numbers of metastatic nodules in the livers were significantly reduced in mice injected with LOVO sh-BMI-1 cells compared with LOVO sh-Control cells. (B) Number of the metastasis nodules per liver was counted in mice injected with indicated cells ($n = 7$ or 10 per group). (C) Histological BMI-1 and snail staining performed on liver metastasis samples from mice injected with HCT116 sh-Control or HCT116 sh-BMI-1, DLD1 vector or DLD1 BMI-1 cells. Representative images of liver sections are shown. Scale bars, 100 μm . (D) BMI-1 and snail protein expression in mouse livers of different groups was assessed by Western blot analysis. GAPDH was used as a control.

also accordingly reduced after NaB treatment (Fig. 6C and D). Therefore, these data demonstrate that inhibition of BMI-1 expression in CRC cells by NaB reduced CRC liver metastasis.

4. Discussion

Previous researches have demonstrated that BMI-1 promotes tumorigenesis and cancer progression in several cancers including CRC, prostate cancer, breast cancer^{18–20}. However, the role of BMI-1 in CRCLM has not been elucidated. Our present study provides clinic evidence that BMI-1 was overexpressed in the tissues of primary CRC compared with adjacent non-cancerous tissues. This is in agreement with previous reports^{6–8}. Interestingly, the expression level of BMI-1 in liver metastases (but not lymph node metastases) was dramatically upregulated compared with primary CRC tissues. BMI-1 expression level in primary CRC tissue was only significantly associated with BMI-1 expression level in liver metastases, thus we proposed that RNA

or protein of BMI-1 in CRC tissues could be used to predict the risk of liver metastases from CRC. Using a series of *in vitro* and *in vivo* assays, we provided evidences that BMI-1 enhances migration ability in CRC cells and liver metastases in mice. These results support a significant oncogenic role of BMI-1 in CRCLM through promoting CRC cell migration.

The prognostic significance of BMI-1 expression in CRC tissues is conflicting. Several studies reported that the overexpression of BMI-1 protein in CRC was associated with tumor recurrence or metastasis and lower survival rate of the patients than that in patients with low expression^{6–8}. However, other study reported high BMI-1 expression was correlated with a better prognosis compared to patients with low expression²¹. In this study, we found that BMI-1 expression level in liver metastases was significantly higher in T4 stage compared with T3 stage CRC patients, and was associated with invasion depth and right-sided primary tumor. Though CRC originating from right-sided cancers (ascending colon, transverse colon, cecum) had a lower incidence of liver metastases than that of left-sided cancers

(descending colon, sigmoid colon, rectum), clinical studies showed worse survival and lower resection rates in liver metastatic right-sided CRC patients^{22–24}. Higher BMI-1 expression in liver metastases from right-sided tumor may explain the inferior survival of right-sided CRC that observed in patients with CRCLM.

EMT was initially used in the process of embryogenesis. As for tumorigenesis, EMT is closely related to tumor invasion and migration²⁵. Increasing evidence indicates that dysregulation of EMT triggered cancer metastasis²⁶. The study of Song et al.²⁷ firstly clarified the essentiality of BMI-1 in inducing EMT by stabilization of snail *via* PI3K/AKT/GSK-3 β pathway in nasopharyngeal carcinoma cells. Then, in some malignant tumors, BMI-1 was demonstrated to induce EMT^{20,28}. Herein, we apply four CRC cell lines to test the effect of BMI-1 in regulating metastasis and EMT phenotype of CRC cells. In two high

metastatic cells, HCT116 and LOVO, downregulation of BMI-1 inhibited cell migration rate and EMT phenotype. In two low metastatic cells, the result is just the opposite. In order to investigate the molecular mechanism underlay these results, we focused on AKT/GSK-3 β /snail signaling. Previous studies revealed that AKT/GSK-3 β /snail signaling is the critical pathway of EMT process²⁹. GSK-3 is an important downstream regulator of PI3 kinase/AKT pathway, and its activity can be suppressed by AKT-mediated phosphorylation at Ser9 of GSK-3 β ^{30,31}. Our data show that the change of BMI-1 expression influenced the phosphorylation of GSK-3 β through regulating phosphorylation of AKT, rather than the total amount of GSK-3 β . This phenomenon can be reversed by PI3K inhibitor wortmannin. Snail is reported to be dually regulate by GSK-3 β ³². It promoted EMT by acting on E-cadherin³³. In our study, wortmannin can reverse the expression of

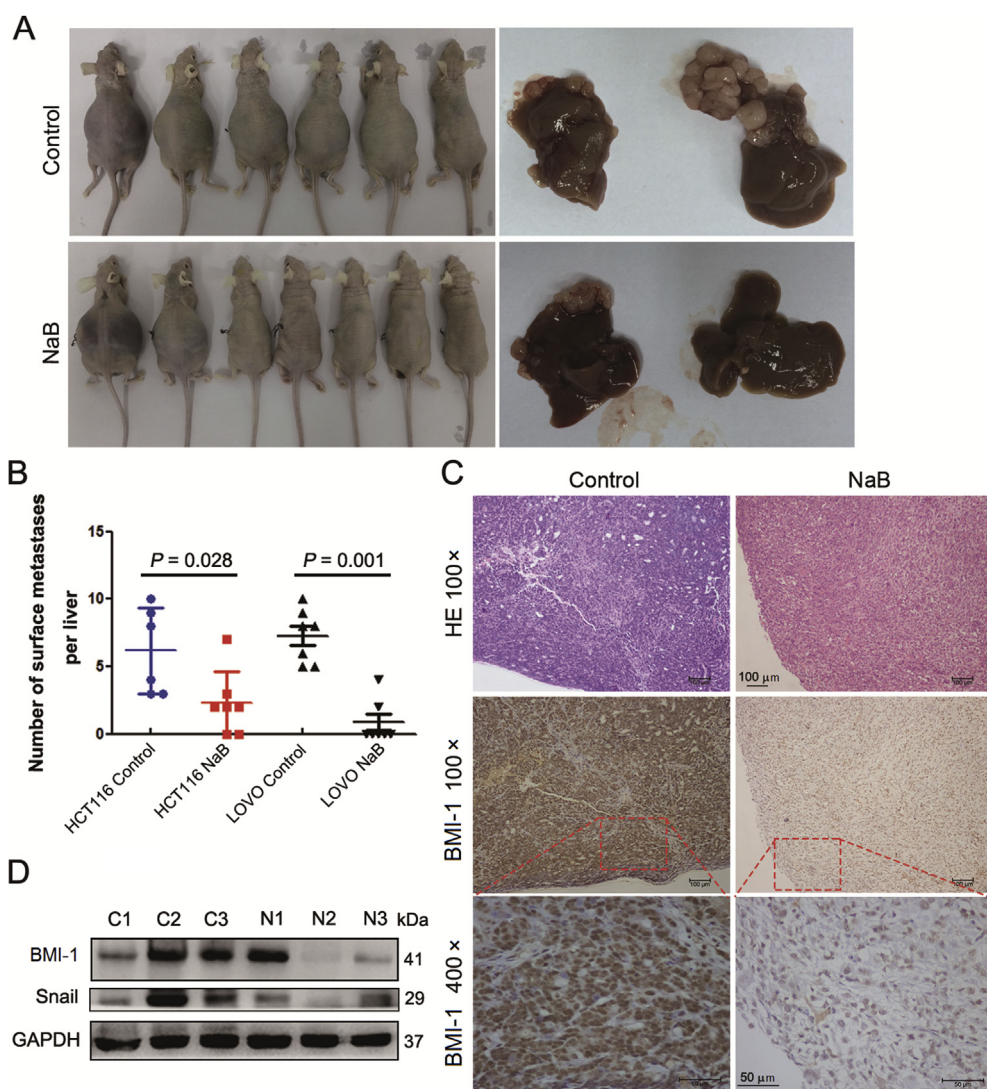


Figure 6 NaB inhibited CRC liver metastasis *in vivo*. (A) NaB treatment reduced liver metastasis and malignant ascites in mice injected with HCT116 cells ($n = 6$ or 7 per group). Three weeks after injection of HCT116 cells into the spleens of athymic nude mice, animals were killed and livers were examined for metastatic nodules. (B) Number of the metastasis nodules per liver was counted in mice injected with HCT116 or LOVO cells with/without NaB treatment ($n = 6$ or 7 per group). NaB treatment significantly reduced the number of liver metastases. (C) Histological BMI-1 staining performed on liver metastasis samples from mice injected with LOVO cells with/without NaB treatment. Representative images of liver sections are shown at $100\times$ and $400\times$ magnification, respectively (Scale bar: $50\ \mu\text{m}$). (D) Western blot analysis of BMI-1 and snail protein expression in livers of mice injected with LOVO cells with/without NaB treatment. GAPDH was used as a control.

snail and E-cadherin under the regulation of BMI-1. Moreover, we clarified that snail plays a role in BMI-1-mediated metastasis in CRC by establishing sh-*BMI-1*/snail and *BMI-1*/sh-snail CRC cell lines. Furthermore, the mRNA and protein expression levels of BMI-1 and snail were positive correlated in primary CRC tissues and paired liver metastases. IHC and Western blot results also confirmed that the expression levels of BMI-1 and snail were reduced in HCT116 sh-*BMI-1* cells injected mice livers, and increased in DLD1 *BMI-1* cells injected mouse livers. Thus, we come up with a conclusion that BMI-1 can promote EMT of CRC through AKT/GSK-3 β /snail pathway.

NaB is one of short-chain fatty acids naturally occurred by human colonic flora³⁴. It's also a kind of HDACi which transcriptionally repress lots of oncogenes, such as *BMI-1*^{16,35,36}. HDACi were proven to have potent anticancer activity³⁷. In our previous study, we found that NaB inhibited CRC cell migration through inhibiting the expression of BMI-1¹⁷. Here we show that downregulation of BMI-1 by NaB inhibited human CRC cells liver metastasis in nude mice. In our other study, we found that NaB inhibited CT26 mice colon cell induced CRCLM *in vivo*³⁸. Therefore, our data suggest that NaB will be considered as a potential treatment for inhibiting CRCLM.

5. Conclusions

Our study has shown the biological and clinical significance of BMI-1 in CRCLM. BMI-1 facilitates CRC cells migration through EMT by modulating AKT/GSK-3 β /snail signaling pathway. Besides, NaB, which is one of BMI-1 inhibitors, suppresses CRC cells migration and inhibits CRCLM *in vivo*. Hence, a therapeutic intervention that interrupts the functional interplays between BMI-1 and AKT/GSK-3 β /snail signaling might provide a potential treatment for CRCLM.

Acknowledgments

This work was supported by the National Natural Science Foundation of China (Nos. 81272493 and 81472213), the Health Commission of Zhejiang Province (Nos. 2019331258 and 2019335600, China), Natural Sciences Foundation of Zhejiang Province (No. LY17H220001, China), the Science Technology Department of Zhejiang Province (Nos. LGF20H220001 and 2015C37112, China). We thank Dr. Hui Liu for statistical analysis.

Author contributions

Guanyu Wang and Qinghua Dong conceived and designed this research. Zhiyao Xu, Zhuha Zhou, Jing Zhang, Feichao Xuan, Zhenyu Liuyang, Mengjing Fan, Difan Zhou, Ximei Ma, Yiyang Hong and Yihong Wang performed the experiments. Guanyu Wang, Qinghua Dong, Sherven Sharma, Zhiyao Xu and Zhuha Zhou contributed to data interpretation and wrote the manuscript. All authors read and approved the final manuscript.

Conflicts of interest

The authors declare no conflicts of interest.

Appendix A. Supporting information

Supporting data to this article can be found online at <https://doi.org/10.1016/j.apsb.2020.11.018>.

References

1. Siegel RL, Miller KD, Goding Sauer A, Fedewa SA, Butterly LF, Anderson JC, et al. Colorectal cancer statistics, 2020. *Ca-Cancer J Clin* 2020;**70**:1–30.
2. Bray F, Ferlay J, Soerjomataram I, Siegel RL, Torre LA, Jemal A. Global cancer statistics 2018: GLOBOCAN estimates of incidence and mortality worldwide for 36 cancers in 185 countries. *Ca-Cancer J Clin* 2018;**68**:394–424.
3. Valderrama-Treviño AI, Barrera-Mera B, Ceballos-Villalva JC, Montalvo-Javé EE. Hepatic metastasis from colorectal cancer. *Euroasian J Hepatogastroenterol* 2017;**7**:166–75.
4. Jacobs JJ, Kieboom K, Marino S, DePinho RA, van Lohuizen M. The oncogene and polycomb-group gene *Bmi-1* regulates cell proliferation and senescence through the ink4a locus. *Nature* 1999;**397**:164–8.
5. Tateishi K, Ohta M, Kanai F, Guleng B, Tanaka Y, Asaoka Y, et al. Dysregulated expression of stem cell factor *Bmi1* in precancerous lesions of the gastrointestinal tract. *Clin Canc Res* 2006;**12**:6960–6.
6. Li DW, Tang HM, Fan JW, Yan DW, Zhou CZ, Li SX, et al. Expression level of *Bmi-1* oncoprotein is associated with progression and prognosis in colon cancer. *J Canc Res Clin Oncol* 2010;**136**:997–1006.
7. Kim JH, Yoon SY, Kim CN, Joo JH, Moon SK, Choe IS, et al. The *Bmi-1* oncoprotein is overexpressed in human colorectal cancer and correlates with the reduced p16INK4a/p14ARF proteins. *Canc Lett* 2004;**203**:217–24.
8. Alajez NM. Significance of BMI1 and FSCN1 expression in colorectal cancer. *Saudi J Gastroenterol* 2016;**22**:288–93.
9. Zhang X, Yang X, Zhang Y, Liu X, Zheng G, Yang Y, et al. Direct serum assay for cell-free *Bmi-1* mRNA and its potential diagnostic and prognostic value for colorectal cancer. *Clin Canc Res* 2015;**21**:1225–33.
10. Pun JC, Chan JY, Chun BK, Ng KW, Tsui SY, Wan TM, et al. Plasma *Bmi1* mRNA as a potential prognostic biomarker for distant metastasis in colorectal cancer patients. *Mol Clin Oncol* 2014;**2**:817–20.
11. Maynard MA, Ferretti R, Hilgendorf KI, Perret C, Whyte P, Lees JA. *Bmi1* is required for tumorigenesis in a mouse model of intestinal cancer. *Oncogene* 2014;**33**:3742–7.
12. He X, Dong Y, Wu CW, Zhao Z, Ng SS, Chan FK, et al. MicroRNA-218 inhibits cell cycle progression and promotes apoptosis in colon cancer by downregulating BMI1 polycomb ring finger oncogene. *Mol Med* 2013;**18**:1491–8.
13. Lim B, Mun J, Kim JH, Kim CW, Roh SA, Cho DH, et al. Genome-wide mutation profiles of colorectal tumors and associated liver metastases at the exome and transcriptome levels. *Oncotarget* 2015;**6**:22179–90.
14. Liu L, Dai Y, Chen J, Zeng T, Li Y, Chen L, et al. Maelstrom promotes hepatocellular carcinoma metastasis by inducing epithelial–mesenchymal transition by way of Akt/GSK-3 β /Snail signaling. *Hepatology* 2014;**59**:531–43.
15. Losson H, Schnekenburger M, Dicato M, Diederich M. Natural compound histone deacetylase inhibitors (HDACi): synergy with inflammatory signaling pathway modulators and clinical applications in cancer. *Molecules* 2016;**21**:1608.
16. Bommi PV, Dimri M, Sahasrabudhe AA, Khandekar J, Dimri GP. The polycomb group protein BMI1 is a transcriptional target of HDAC inhibitors. *Cell Cycle* 2010;**9**:2663–73.
17. Xu Z, Tao J, Chen P, Chen L, Sharma S, Wang G, et al. Sodium butyrate inhibits colorectal cancer cell migration by downregulating *Bmi-1* through enhanced miR-200c expression. *Mol Nutr Food Res* 2018;**62**:e1700844.

18. Liu X, Wei W, Li X, Shen P, Ju D, Wang Z, et al. BMI1 and MEL18 promote colitis-associated cancer in mice *via* REG3B and STAT3. *Gastroenterology* 2017;**153**:1607–20.
19. Zhu S, Zhao D, Yan L, Jiang W, Kim JS, Gu B, et al. BMI1 regulates androgen receptor in prostate cancer independently of the polycomb repressive complex 1. *Nat Commun* 2018;**9**:500.
20. Janaki Ramaiah M, Vaishnave S. BMI1 and PTEN are key determinants of breast cancer therapy: a plausible therapeutic target in breast cancer. *Gene* 2018;**678**:302–11.
21. Benard A, Goossens-Beumer IJ, van Hoesel AQ, Horati H, Putter H, Zeestraten EC, et al. Prognostic value of polycomb proteins EZH2, BMI1 and SUZ12 and histone modification H3K27me3 in colorectal cancer. *PLoS One* 2014;**9**:e108265.
22. Engstrand J, Nilsson H, Strömberg C, Jonas E, Freedman J. Colorectal cancer liver metastases—a population-based study on incidence, management and survival. *BMC Canc* 2018;**18**:78.
23. Price TJ, Beeke C, Ullah S, Padbury R, Maddern G, Roder D, et al. Does the primary site of colorectal cancer impact outcomes for patients with metastatic disease. *Cancer* 2015;**121**:830–5.
24. Van der Pool AE, Damhuis RA, Ijzermans JN, de Wilt JH, Eggermont AM, Kranse R, et al. Trends in incidence, treatment and survival of patients with stage IV colorectal cancer: a population-based series. *Colorectal Dis* 2012;**14**:56–61.
25. De Craene B, Berx G. Regulatory networks defining EMT during cancer initiation and progression. *Nat Rev Canc* 2013;**13**:97–110.
26. Aiello NM, Kang Y. Context-dependent EMT programs in cancer metastasis. *J Exp Med* 2019;**216**:1016–26.
27. Song LB, Li J, Liao WT, Feng Y, Yu CP, Hu LJ, et al. The polycomb group protein Bmi-1 represses the tumor suppressor PTEN and induces epithelial–mesenchymal transition in human nasopharyngeal epithelial cells. *J Clin Invest* 2009;**119**:3626–36.
28. Yang MH, Hsu DS, Wang HW, Wang HJ, Lan HY, Yang WH, et al. Bmi1 is essential in Twist1-induced epithelial–mesenchymal transition. *Nat Cell Biol* 2010;**12**:982–92.
29. Lan Y, Han J, Wang Y, Wang J, Yang G, Li K, et al. STK17B promotes carcinogenesis and metastasis *via* AKT/GSK-3 β /Snail signaling in hepatocellular carcinoma. *Cell Death Dis* 2018;**9**:236.
30. Srivastava AK, Pandey SK. Potential mechanism(s) involved in the regulation of glycogen synthesis by insulin. *Mol Cell Biochem* 1998;**182**:135–41.
31. Cross DA, Alessi DR, Cohen P, Andjelkovich M, Hemmings BA. Inhibition of glycogen synthase kinase-3 by insulin mediated by protein kinase B. *Nature* 1995;**378**:785–9.
32. Zhou BP, Deng J, Xia W, Xu J, Li YM, Gunduz M, et al. Dual regulation of Snail by GSK-3 β -mediated phosphorylation in control of epithelial–mesenchymal transition. *Nat Cell Biol* 2004;**6**:931–40.
33. Cano A, Pérez-Moreno MA, Rodrigo I, Locascio A, Blanco MJ, del Barrio MG, et al. The transcription factor snail controls epithelial–mesenchymal transitions by repressing E-cadherin expression. *Nat Cell Biol* 2000;**2**:76–83.
34. Louis P, Flint HJ. Diversity, metabolism and microbial ecology of butyrate-producing bacteria from the human large intestine. *FEMS Microbiol Lett* 2009;**294**:1–8.
35. Pant K, Yadav AK, Gupta P, Islam R, Saraya A, Venugopal SK. Butyrate induces ROS-mediated apoptosis by modulating miR-22/SIRT-1 pathway in hepatic cancer cells. *Redox Biol* 2017;**12**:340–9.
36. Xiao X, Cao Y, Chen H. Profiling and characterization of microRNAs responding to sodium butyrate treatment in A549 cells. *J Cell Biochem* 2018;**119**:3563–73.
37. Huang YH, Chen SQ, Wu SC, Dong GQ, Sheng CQ. Evodiamine-inspired dual inhibitors of histone deacetylase 1 (HDAC1) and topoisomerase 2 (TOP2) with potent antitumor activity. *Acta Pharm Sin B* 2020;**10**:1294–308.
38. Ma X, Zhou Z, Zhang X, Fan M, Hong Y, Feng Y, et al. Sodium butyrate modulates gut microbiota and immune response in colorectal cancer liver metastatic mice. *Cell Biol Toxicol* 2020;**36**:509–15.